VNU Journal of Science: Mathematics - Physics

Journal homepage: https://js.vnu.edu.vn/MaP

Original Article

Pressure-induced Glassy Networks of Enstatite ($MgSiO_3$) and Forsterite (Mg_2SiO_4)

Nguyen Hoang Anh[1, 2,*], Nguyen Hung Son[1], Nguyen Van Hong[1]

[1]*Hanoi University of Science and Technology, 1 Dai Co Viet, Hanoi, Vietnam*

[2]*International Center for Theoretical Physics, 11 Strada Costiera, Trieste 34151, Italy*

Received 15 July 2022
Revised 5 September 2022; Accepted 11 October 2022

Abstract: This work is designed to focus on the glassy network analysis and visualizing the cluster and subnets formation, the rich set of bond-, edge- and face-sharing linkages. The correlation between the degree of polymerization and linkages forming is apparently indicated. The distribution of SiO_x clusters is computed to determine the polymerization characteristic and Mg-rich region. The distribution of BOs, NBOs and FOs also are investigated to prove the behavior of Mg^{2+} incorporating into the -Si-O- network. Polyhedral units, clusters, and subnets are vividly visualized so as to have a better understanding of cluster merging. Besides, in this work we have also clarified the distribution of edge-sharing and face-sharing subnets/network between Si-Si and Mg-Si species.

Keywords: $MgSiO_3$, Mg_2SiO_4, pressure change, glassy network, cluster merging.

1. Introduction

The SiO_2-based materials are the main components of the Earth's mantle. They have the versatile characteristics to be applied in high-technology fields. Therefore, deep-sighted investigations on these materials have happened for a long time [1-6]. Previous works indicated that silica has a random continuous network which is built by SiO_4 units at ambient pressure [7]. When MgO component is doped into SiO_2, Mg then acts as the network modifier and network former [8, 9]. Mg^{2+} ions break the glassy network, forming non-bridging and free oxygen. The fractions of generated BO and FO depend on the content of MgO doped into the SiO_2 [10].

* Corresponding author.
E-mail address: hoanganhnguyen.vietnam@gmail.com

https//doi.org/10.25073/2588-1124/vnumap.4767

In $MgSiO_3$, the mean bond distance of Si-O, O-O, Mg-O and Si-Si are 1.60, 2.61, 1.93 and 3.08 Å, one to one [11]. The coordination number of Si-O and Mg-O are 4 and 4.1, respectively. In terms of angle distribution, Haskins showed that the O-Si-O is normally distributed around 108° (~109.5 °) [12]. Therefore, the SiO_4 units in $MgSiO_3$ are nearly perfectly tetrahedrons [13]. The mean O-Mg-O angle in $MgSiO_3$ is smaller than the one in MgO, and has bimodal distribution [12]. By molecular dynamics simulation, the study on $(MgO)_x(SiO_2)_{100-x}$ (x = 50, 54, 58, 62, 67) showed that the coordination number of Mg increases from 4.5 ± 0.3 to 5.0 ± 0.3 as x increases from 50 to 67 [14]. The Si-O bond length (R_{Si-O}) insignificantly changes under the content of MgO in the material. The O-O coordination number decreases from 6.00 in vitreous silica to 4.00 in forsterite (Mg_2SiO_4).

To clarify the intermediate-range order of v-Mg_2SiO_4, Kohara et al. indicated that Q^n distribution is employed [15]. Q^0 and Q^1 are dominant at ambient pressure. Q^2, Q^3 and Q^4 exist in small proportions. Therefore, v-Mg_2SiO_4 compound is extremely fragile. Besides, the average Si-O and Mg-O coordination number correspondingly are 4.5 ± 0.1 Å and 4.95 Å. In the analysis of T(r), the Mg-O distribution is in the range of 1.8-2.5 Å because of distorted MgO_x units. That Mg-O peak has a bulge at the high-r side.

In addition to investigation at ambient pressure, $MgSiO_3$ and Mg_2SiO_4 characteristics are also clarified under compression. By using high-energy X-ray diffraction, Benmore et al. indicate that the mean bond length of Si-O slightly decreases from 0 to 10 GPa [16]. This phenomenon is happed in SiO_2 [17]. However, at pressures beyond 15 GPa, the Si-O bond length increases. The Mg-O bond length decreases from 2.0 Å at 0 GPa to 1.91 ± 0.01 Å at 30 GPa.

Under compression, the polymerization of Mg_2SiO_4 changes strongly [18]. With the increase of pressure, corner-, edge-, and face-sharing linkages increase. Their spatial distributions are not uniform but they have the tendency to form clusters. Besides, the SiO_x units also tend to merge under pressure. To have a better understanding of the effect of the MgO on glassy formation, we have carried-out the investigation on $MgSiO_3$ and Mg_2SiO_4 and put forward the intuitive visualization of the glassy network formation.

2. Methodology

Both $MgSiO_3$ consisting of 5,000 atoms and Mg_2SiO_4 consisting of 4,998 atoms are constructed by molecular dynamics simulations at 600 K and in the pressure range of 0 – 100 GPa. The OG potential which is successful to build SiO_2-based components is employed in this work. The Buckingham form of Oganov potential function is presented as:

$$\varphi_{ij}(r_{ij}) = \frac{q_i q_j e^2}{4\pi r_{ij}} + A_{ij} \exp\left(-\frac{r_{ij}}{B_{ij}}\right) - \frac{C_{ij}}{r_{ij}^6}$$

where, q_i and q_j are effective charges of i^{th} and j^{th} atom, one to one; r_{ij} are distance between i^{th} and j^{th} atom, e is the electron charge and A_{ij}, B_{ij} and C_{ij} are parameters presenting the repulsive and attractive van der Waals forces [19-23]. The parameters with a value different from 0 of Oganov potential are listed in Table 1. Verlet algorithm is used with time step Δt is 0.47 fs. First, atoms are randomly seeded within the periodical box. The box is heated to a high temperature with the purpose of completely removing the initial configuration. We, then, quenched the model to 5,000 K; 4,000 K; 3,500 K within 10,000-time steps with the quenching speed being 2.5 K/ps. At each temperature, the model is relaxed to assure it is not broken. After that, we compress the models to pressures of 5, 10, 15, 20, 25, 30, 40, 60, 80, and 100 GPa. These 11 models, including 0 GPa model, are cooled down to 600 K and relaxed for 100,000-time steps by NPT (number of atoms, pressure and temperature are constant) procedure. Finally, the analysis is performed by averaging the characteristics of the last 5,000 models.

Table 1. Parameters of OG potential

Pair potential parameter	Value	Unit
A_{O-O}	1.952624×10^5	kJ/mol
B_{O-O}	0.02674	nm
C_{O-O}	3.189199×10^{-4}	kJ nm^6/mol
A_{Si-O}	1.097039×10^5	kJ/mol
B_{Si-O}	0.02827	nm
A_{Mg-O}	1.004808×10^5	kJ/mol
B_{Mg-O}	0.02866	nm

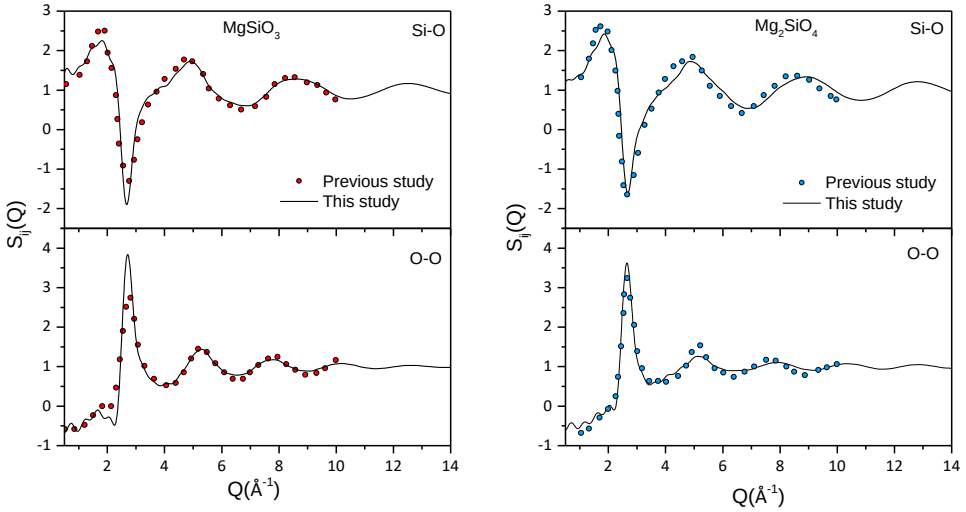

Figure 1. Partial structure factors of Si-O, O-O and Si-Si pairs. The solid lines are results obtained from this study, dots are results extracted from RMC method [24].

Table 2. The comparison of the structural properties in $MgSiO_3$ and Mg_2SiO_4 between our work and the other ones (both simulation and experiment method). Assign Z is coordination number, d is the bond distance

Type	Z_{Si-O}	Z_{Mg-O}	d_{Si-O}	d_{Mg-O}
This study	4.1	4.3	1.60	1.86
Wilding et al., [25]	4.0	4.5	1.64	2.00
Kubicki et al., [26]	4.0	4.3	1.59	1.90
Yin et al., [11]	4.1	4.1	1.63	2.08
This study	4.0	4.8	1.58	1.96
Wilding et al., [25]	4.0	5.1	1.64	2.00
Kohara et al., [15]	4.05	4.95	1.60	2.00
Kohara et al., [27]	4.0	5.3	1.60	

The coordination number of Si-O and Mg-O at zero pressure, respectively is of 4.1 and 4.3 for $MgSiO_3$, andis of 4.0 and 4.8 for Mg_2SiO_4. To demonstrate the robustness of the obtained results, the comparison of the structural characteristics (average bond length and corresponding coordination

number) of $MgSiO_3$ and Mg_2SiO_4 models between this work and previous studies are apparently presented in Table 2, there is a good agreement between them. In other words, the models in this study are generated successfully and completely reliable.

3. Results and Discussion

3.1. Local Structure of Fundamental Units in $MgSiO_3$ and Mg_2SiO_4 under Compression

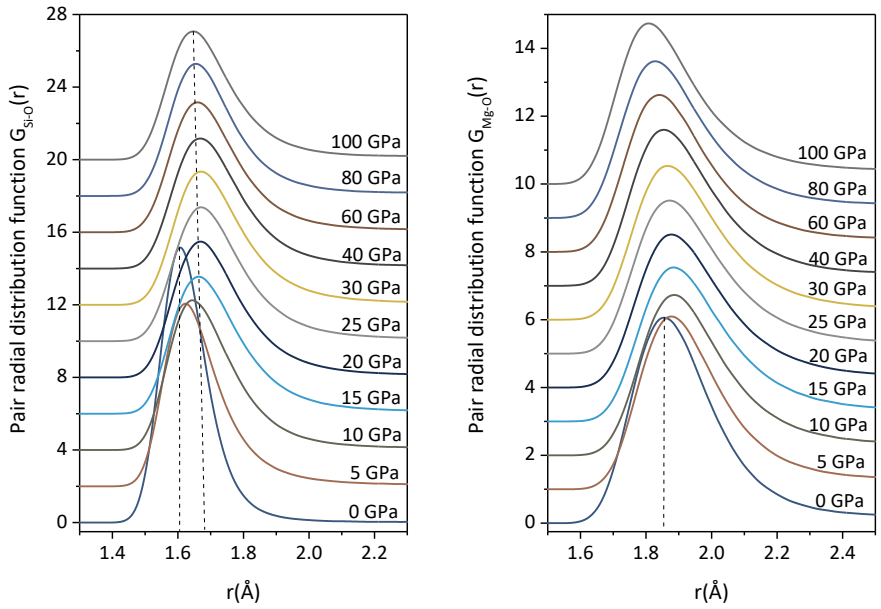

Figure 2. Pair radial distribution function of Si-O and Mg-O pairs at different pressure in $MgSiO_3$.

The pair radial distribution function (PRDF) of Si-O and Mg-O have been illustrated in Figure 2 for $MgSiO_3$. It can be obviously interpreted that the position of the first peak in Si-O PRDF is ~ 1.60 -1.65 Å in the 0 – 15 pressure range. At 15 GPa upward, the PRDF marginally shifts to the right (approximately 1.70 Å at 40 GPa). Then, the first peak location tends to reduce by 0.20 Å. Whereas, at pressure interval (0-15), the peak location of Si-O PRDFs of Mg_2SiO_4 virtually plateaus in the same position (right under 1.60 Å) (see Figure 3). At higher pressure, the Si-O PRDFs in Mg_2SiO_4 depend substantially on pressure and have a tendency of changing like in $MgSiO_3$ (maximal length reaches 1.65 Å at 40 GPa). In contrast, the first peak position of Mg-O tends to shift to the left in $MgSiO_3$ and Mg_2SiO_4 models under densification. In the corresponding pressure of 0 GPa and 100 GPa, the first peak position is located at 1.86 Å and 1.80 Å for $MgSiO_3$, 1.96 Å and 1.85 Å for Mg_2SiO_4. As we can see in Figure 2, at ambient pressure, the first peak of Si-O PRDFs has a sharp shape, this elucidates that the local structure of magnesium silicate at 0 GPa is more ordered than one at high pressure. Both positions of Si-O peak in $MgSiO_3$ and Mg_2SiO_4 components shift to the right and (0 – 40 GPa range) then shift slightly to the left at beyond pressures while the height decreases. That is attributed to the formation of SiO_x units (x=5,6,7,…) at high pressure. The relevant snapshots are shown in Figure 4. This issue also has been clarified by Nhan et al., [28]. The mean bond length of Si-O in SiO_6 unit is longer than the one in SiO_5, and the one in SiO_4 is the shortest one, while the numbers of SiO_6 and SiO_5 units increase under compression. As a result, the first peak of Si-O PRDF tends to shift to the right; it means the average

bond length of Si-O in SiO_x increases. At the higher pressure, SiO_5 and SiO_6 units are still formed, but the bond lengths of Si-O in those units decrease because of the strong compression. In the meanwhile, this decline is faster than the increase in mean bond length caused by the formation of SiO_5 and SiO_6 units. Therefore, it could be said that the mean bond length of Si-O in SiO_x units decreases.

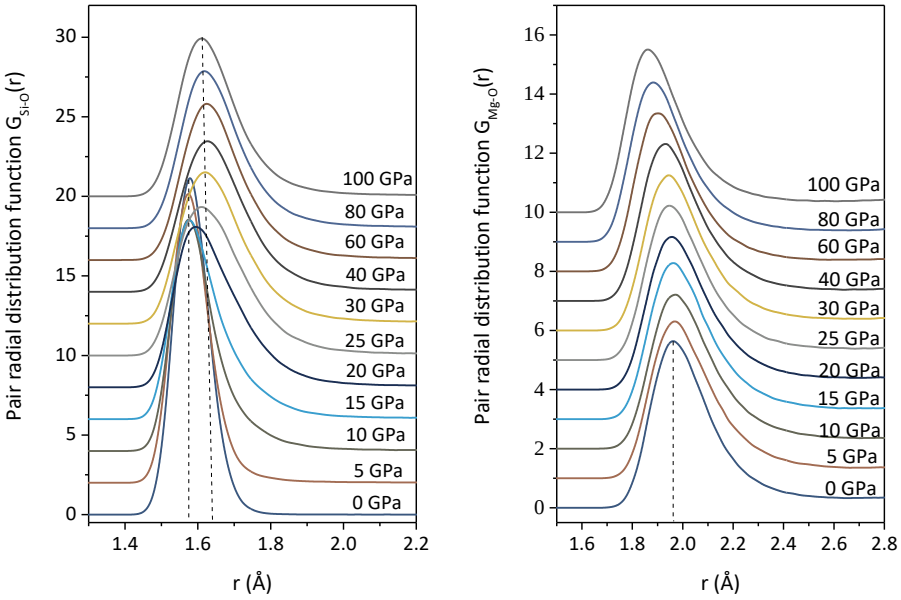

Figure 3. Pair radial distribution function of Si-O and Mg-O pairs at different pressure in Mg_2SiO_4.

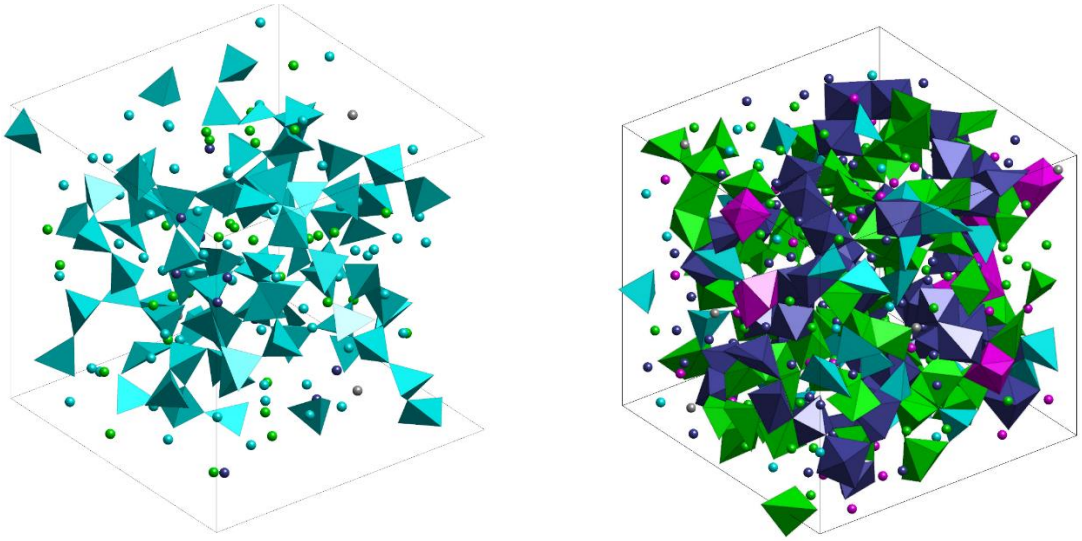

a) 0 GPa b) 20 GPa

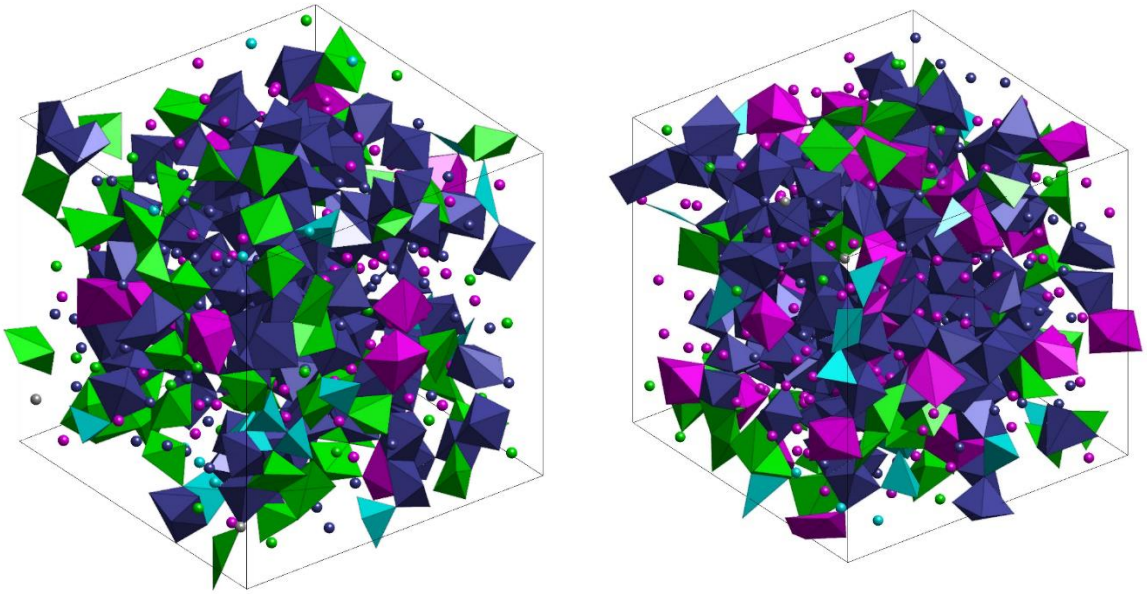

c) 60 GPa d) 100 GPa

Figure 4.Envision snapshots of MgSiO3 glass structures at four different pressures with 585 atoms – 0 GPa, 900 atoms – 20 GPa, 1015 atoms – 60 GPa and 1115 atoms – 100 GPa (in the same cubic size). The Mg (spheres) atoms and Si-O coordinated polyhedron are color-coded to denote the coordination number, where gray represents for threefold, cyan for fourfold, green for fivefold, dark blue for sixfold and magenta for sevenfold or higher.

3.2. Linkage Formation under Compression

To clarify the glassy network in MgO-SiO and 2MgO-SiO glass, the distribution of corner-, edge-, and face-sharing bonds are investigated at different pressures. Table 3 shows the number of the corner-sharing bonds (N_c), edge-sharing bonds (N_e) and face-sharing bonds (N_f) per Si atoms in both $MgSiO_3$ and Mg_2SiO_4. The number of corner-sharing bonds per the number of Si atoms in $MgSiO_3$ is about twice as many as in Mg_2SiO_4 at zero pressure. In addition to the increase of corner-sharing bonds, the edge-sharing and face-sharing bonds gradually appear. The number of corner-sharing bonds per Si atom of $MgSiO_3$ and Mg_2SiO_4 is expressed as a function of pressure. N_c (number of corner-sharing bonds) is dominant; meanwhile, N_e and N_f (number of edge- and face-sharing bonds) take up very small ratios. N_f even has zero value at the bottom range of pressure and reaches the same maximum value of 0.04 in both compositions. The appearance of face-sharing and edge-sharing bonds renders the structural heterogeneity formed. Table 4 evinces the mean bond length of corner-, edge-, and face-sharing bonds. Under compression, the bond length between SiO_x units via corner-sharing bonds changes in the range from 3.10 Å to 3.17 Å in $MgSiO_3$. Meanwhile, in Mg_2SiO_4, those values fluctuate in 3.06 Å to 3.11 Å, which is considerably longer than other linkages. The change of corner-sharing bond length is tight related to the position of the pronounced peak of Si-Si PRDF. In general, all average bond lengths of linkages reduce slightly under tension. As we see, at low pressure, the mean bond length of linkages in $MgSiO_3$ and Mg_2SiO_4 tends to increase. This phenomenon is due to the distribution of mean bond length in SiO_x-polyhedral units. At low pressure (0 to 5 GPa for $MgSiO_3$), the recorded FBL is not a number (NaN), because edge-sharing and face-sharing bonds do not exist in the analyzed model. The evolution of edge-sharing and face-sharing bonds in Mg_2SiO_4 seems to be harder than in $MgSiO_3$ because of the

proportion of constituents in the material. At 0 GPa, the edge-sharing bond is even not found. To depict the formation of different types of linkages, Figure 5 displays the spatial distribution of corner-, edge-, and face-sharing bonds of SiO_x units at pressures (0, 20, 60 and 100 GPa) in Mg_2SiO_4 models.

Table 3. The number of the corner-sharing bonds (N_c), edge-sharing bonds (N_e) and face-sharing bonds (N_f) among SiO_x units per Si atoms in $MgSiO_3$ and Mg_2SiO_4 compounds, at different pressures

P (GPa)	$MgSiO_3$			Mg_2SiO_4		
	N_c	N_e	N_f	N_c	N_e	N_f
0	1.34	0.02	0.00	0.68	0.00	0.00
5	1.61	0.15	0.00	0.75	0.01	0.00
10	1.85	0.29	0.00	0.89	0.04	0.00
15	1.98	0.44	0.01	0.97	0.07	0.00
20	2.01	0.51	0.01	1.16	0.09	0.01
25	2.12	0.56	0.01	1.22	0.18	0.01
30	2.08	0.61	0.01	1.28	0.20	0.01
40	2.14	0.67	0.01	1.36	0.25	0.03
60	2.19	0.77	0.02	1.38	0.36	0.02
80	2.23	0.81	0.04	1.43	0.38	0.03
100	2.18	0.96	0.04	1.47	0.40	0.04

Table 4. The average bond length of corner-sharing bond (CBL), edge-sharing bond (EBL) and face-sharing bond (FBL) in $MgSiO_3$ and Mg_2SiO_4 compounds at different pressures

P (GPa)	$MgSiO_3$			Mg_2SiO_4		
	CBL(Å)	EBL(Å)	FBL(Å)	CBL(Å)	EBL(Å)	FBL(Å)
0	3.14	2.85	NaN	3.07	NaN	NaN
5	3.15	2.86	NaN	3.06	2.79	NaN
10	3.16	2.84	2.68	3.09	2.73	2.54
15	3.17	2.86	2.67	3.10	2.75	NaN
20	3.17	2.85	2.61	3.13	2.72	2.62
25	3.16	2.87	2.61	3.15	2.72	2.49
30	3.16	2.83	2.64	3.14	2.72	2.49
40	3.14	2.83	2.60	3.16	2.73	2.48
60	3.12	2.79	2.62	3.14	2.69	2.46
80	3.11	2.77	2.58	3.13	2.65	2.43
100	3.10	2.76	2.61	3.11	2.63	2.41

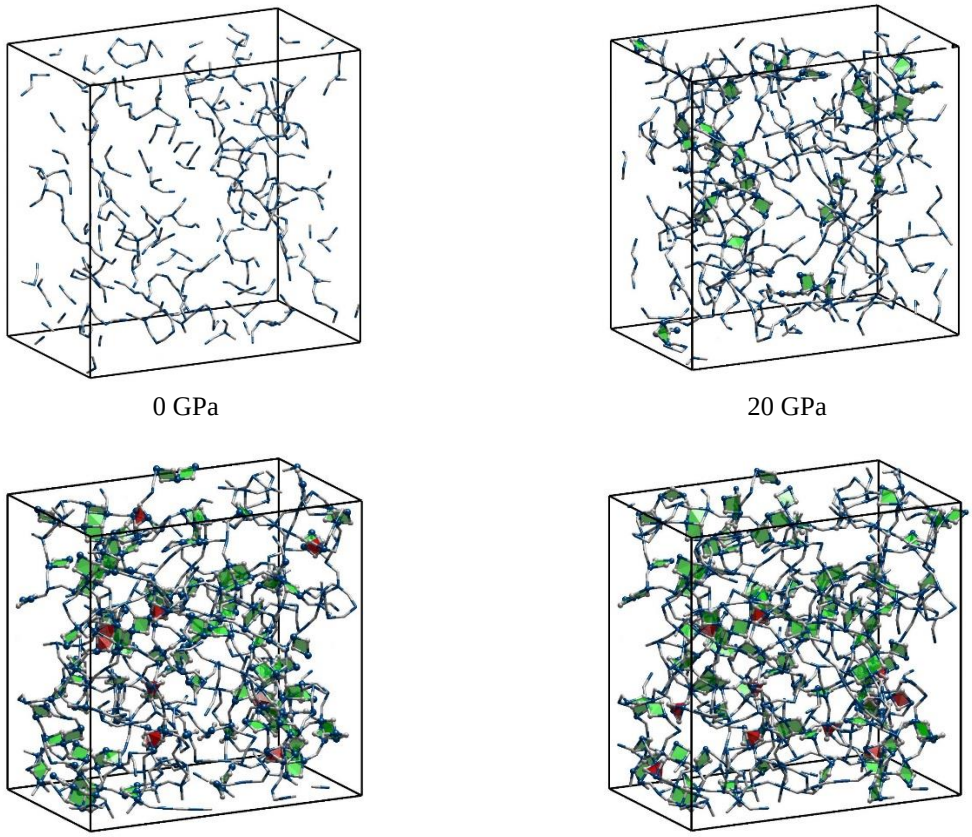

Figure 5. The snapshots of Mg_2SiO_4 model in transition at different considered pressures. Edge-sharing linkages are color-coded by green, face-sharing linkages are presented by red, corner-sharing linkages are polylines.

Table 5. The number of corner-sharing bonds (N_c), edge-sharing bonds (N_e) and face-sharing bonds (N_f) per Si or Mg atoms in $MgSiO_3$ and Mg_2SiO_4 compounds at different pressures

P (GPa)	$MgSiO_3$			Mg_2SiO_4		
	N_c	N_e	N_f	N_c	N_e	N_f
0	1.52	0.26	0.00	1.90	0.16	0.00
5	1.84	0.53	0.02	2.02	0.30	0.00
10	1.86	0.76	0.03	2.03	0.49	0.02
15	1.87	0.93	0.04	2.06	0.62	0.05
20	1.91	1.04	0.05	2.01	0.80	0.10
25	1.76	1.17	0.06	1.97	0.92	0.14
30	1.82	1.16	0.08	1.92	0.98	0.15
40	1.81	1.23	0.11	1.86	1.09	0.20
60	1.79	1.35	0.17	1.81	1.21	0.28
80	1.79	1.43	0.27	1.79	1.24	0.38
100	1.73	1.58	0.31	1.81	1.26	0.43

Table 6. The average bond length of Mg-Si corner-sharing bond (CBL), edge-sharing bond (EBL) and face-sharing bond (FBL) in $MgSiO_3$ and Mg_2SiO_4 compounds at different pressures

P (GPa)	$MgSiO_3$			Mg_2SiO_4		
	CBL(Å)	EBL(Å)	FBL(Å)	CBL(Å)	EBL(Å)	FBL(Å)
0	3.24	2.88	2.67	3.26	2.79	NaN
5	3.24	2.91	2.73	3.26	2.81	2.74
10	3.27	2.92	2.76	3.27	2.84	2.66
15	3.26	2.94	2.74	3.28	2.84	2.66
20	3.27	2.94	2.71	3.30	2.86	2.65
25	3.25	2.93	2.69	3.33	2.86	2.63
30	3.27	2.91	2.71	3.34	2.85	2.64
40	3.27	2.89	2.68	3.34	2.84	2.63
60	3.27	2.86	2.66	3.37	2.82	2.60
80	3.31	2.84	2.65	3.38	2.80	2.57
100	3.33	2.82	2.63	3.37	2.78	2.55

Table 5 and Table 6 evince the number of corner-, edge-, face-sharing bonds per Si or Mg species and the corresponding length between Si and Mg species in $MgSiO_3$ and Mg_2SiO_4. The number of corner-sharing bonds is dominant at low range pressure as the distribution of Si-Si linkages. Considering the range of all pressures, N_e and N_f drastically increase while N_c slightly decreases. N_c gets the maximal value of 1.91 at 20 GPa. At 100 GPa, N_e in $MgSiO_3$ is 1.58 and lower than N_c (1.73). At the high-pressure interval, there are increases in edge-sharing and face-sharing bonds. These linkages have a tendency in forming the cluster/subnet/network. It leads to the appearance of high-density regions because almost TO_x units (T is Mg or Si) linked to each other by edge-sharing or face-sharing bonds mainly have a great coordination number (x=5, 6, 7). The distribution of edge-sharing and face-sharing linkages is not uniform. This is a reason for the structural heterogeneity of the compounds. It means high-density heterogeneity regions appear at the high-pressure interval. The above analysis proves that Mg^{2+} ions link to the glassy network via a common O^{2-} ion at low pressure. Because of the forming of edge-sharing and face-sharing bonds at high pressure, Mg^{2+} ions link to -O-Si- network via all corner-, edge- and face-sharing bonds.

This investigation also indicates the degree of polymerization of $MgSiO_3$ and Mg_2SiO_4 models. To clarify this issue, the distribution of bridging oxygen (BO), non-bridging oxygen (NBO) and free oxygen (FO) under densification is shown in Figure 6. Under compression, the size of the models is shrunk. Therefore, the density of these models increases drastically. The densities of $MgSiO_3$ and Mg_2SiO_4 are about 2.5 and 2.9 g/cm^3 at 0 GPa, and 4.9 and 4.7 g/cm^3 at 100 GPa, respectively. At the highest considered pressure (100 GPa), the density of $MgSiO_3$ is higher. We can realize that the quantities of BOs in $MgSiO_3$ and Mg_2SiO_4 rise strongly in density under 4.0 g/cm^3. When the density is higher than 4.0 g/cm^3, the growth rate of the proportion of BOs becomes slower as the model gets denser. In contrast, the percentages of both NBOs and FOs in $MgSiO_3$, as well as Mg_2SiO_4, reduce gradually in all considered densities. These models have a clear difference in the proportion of various types of oxygen. At all analyzed pressures, FO always accounts for the smallest proportion; meanwhile, the highest ratio swaps between BO and NBO under densification in both compositions. At the 0 GPa (lowest density), the fractions of BO, NBO and FO are 43%, 45% and 12% in $MgSiO_3$; and 18%, 64% and 18% in Mg_2SiO_4, respectively. The ratio of BOs in $MgSiO_3$ is much higher than in Mg_2SiO_4. At densities less than 4.0 (g/cm^3) in both $MgSiO_3$ and Mg_2SiO_4 models, the number of BOs increases, while NBOs and

FOs decrease. At 4.0 (g/cm^3) density, the percentages of BOs, NBOs, FOs are 25%, 70% and 5% in $MgSiO_3$ and 50, 40, and 10% in Mg_2SiO_4 model, respectively. As the density continues to increase, the proportions of all oxygen-types in both models slightly change in the same direction (up and down) at higher range pressure. It means that the fractions in all oxygen-types reach the extreme point at the highest density (highest pressure). In particular, at 100 GPa (4.9 g/cm^3 density in $MgSiO_3$ and 4.7 g/cm^3 in Mg_2SiO_4) the fractions of BOs, NBOs, FOs get the greatest point of 75%, 21% and 4% in $MgSiO_3$, as that of 48%, 43%, and 9% in Mg_2SiO_4, respectively. The number of BOs in $MgSiO_3$ is always larger than that in Mg_2SiO_4 (at the same pressure) due to the variation of Si species content in the systems (1/5 in $MgSiO_3$ and 1/7 in Mg_2SiO_4). The above results once again prove the polymerized characteristic in these ternary systems. According to the distributions of BOs, NBOs and FOs, the intensity of polymerization in $MgSiO_3$ is larger than that in Mg_2SiO_4. In the other words, the fraction of FOs (i.e. oxygen anions do not link to silicon cations) at low pressures takes up a small value, forming a rich region of Mg species. In Mg_2SiO_4, NBOs in the materials account for a considerable percentage. Therefore, we can deduce that the Mg^{2+} ions link to the -Si-O- network via NBOs. Under compression, the percentage of BOs increases while the percentages of NBOs and FOs decrease. As a result, Mg^{2+} ions link to both NBOs and BOs, forming the Mg-glassy network. In $MgSiO_3$, because of the low percentage NBOs at high pressure, Mg^{2+} ions link to the glassy network via mainly BOs.

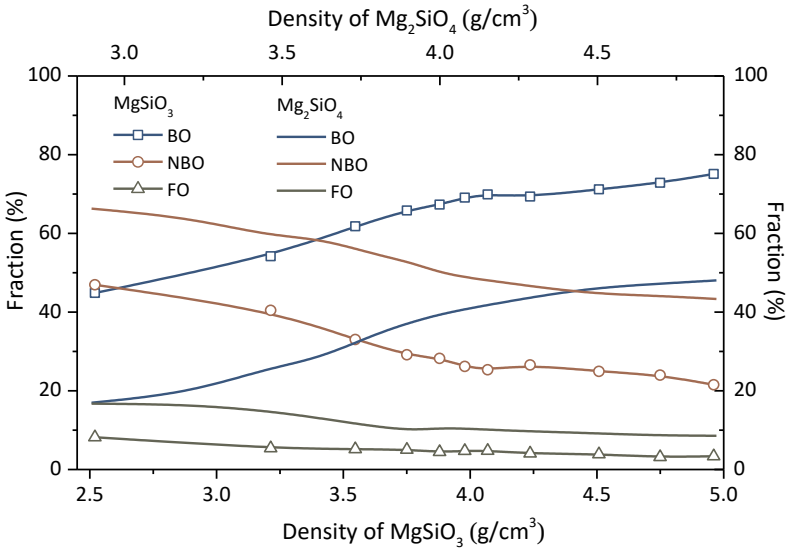

Figure 6. The fractions of BOs, NBOs and FOs under densification, in $MgSiO_3$ and Mg_2SiO_4 models.

3.3. Cluster Merging under Compression

Besides, to point out the degree of polymerization in the glassy composition, the distribution of the Q^n sites is examined in $MgSiO_3$ and Mg_2SiO_4 (see Table 6), where n is the number of bringing oxygen, in the vicinity atom layer; Q is the SiO_x unit. In $MgSiO_3$, the percentage of Q^0 is very small, representing isolated polyhedrons. Q^3 species is the most abundant at ambient pressure and significantly decreases in association with the pressure raise. At the highest pressure, Q^6 accounts for about four-tenths (the greatest proportion), Q^5 is one-fifth, Q^4 is nearly one-tenth, while Q^x (x = 0, 1, 2, 3) is almost 0. Similarly, we can use the information in Table 7 to compare the differences among the Q^n distributions in Mg-SiO glass. At ambient pressure, a mixture of Q^0, Q^1 and Q^2 is dominant (about 80%), while Q^x (x=3,4,5,6)

accounts for a small value, Q^5 and Q^6 are almost zero. Under tension, Q^0, Q^1 and Q^2 reduce substantially, meanwhile, Q^x (x>2) goes up rapidly. At around 10 GPa, the percentage Q^2 gets the highest point of nearly 38%, after that this value goes down substantially. Q^3 reaches the maximum value of approximately 28% at 20 GPa and then reduces to about 15% at 100 GPa. Q^4, Q^5 and Q^6 monotonically increase over the entire pressure range, but the change of Q^6 is the most gradual. At ambient pressure, although there is almost none of Q^4, its growth speed is the strongest during the period of rising pressure. Gradually, Q^4 surpasses Q^3 and becomes the most abundant at 100 GPa. The quantity of Q^0 at the highest pressure is almost 0. Further compressing renders a growth up of high-order species. It means that SiO_x units increase the ability to link to each other in order to create the big subnets. In other words, the degree of polymerization redoubles in both $MgSiO_3$ and Mg_2SiO_4 models. There are differences in the fraction of BOs (see Figure 6) as well as the size distribution of clusters (see Table 8 and Table 9) in the two compounds. Because high-Q species are more dominant in $MgSiO_3$ than in Mg_2SiO_4 at the similar pressure. For instance, at 0 GPa, the most dominant species are Q^3 in $MgSiO_3$ and Q^1 in Mg_2SiO_4.

Table 7. The percentages of calculated abundances of Q^n species in Mg_2SiO_4 glass

$MgSiO_3$							
P (GPa)	Q^0 (%)	Q^1 (%)	Q^2 (%)	Q^3 (%)	Q^4 (%)	Q^5 (%)	Q^6 (%)
0	1.20	10.70	27.30	37.70	20.50	2.60	0.00
5	0.20	3.30	17.20	28.60	33.50	14.50	2.60
10	0.10	1.60	6.60	20.30	32.20	28.50	10.70
15	0.00	0.80	4.80	11.40	26.50	35.50	20.80
20	0.00	0.50	2.80	12.20	24.40	33.10	26.30
25	0.00	0.30	1.80	9.00	21.10	37.20	28.80
30	0.20	0.20	1.70	6.30	19.60	38.30	32.40
40	0.00	0.50	0.90	6.60	19.40	34.60	34.90
60	0.00	0.20	0.40	5.00	15.00	34.50	38.30
80	0.00	0.10	0.40	3.70	13.10	29.60	39.30
100	0.00	0.00	0.30	1.70	9.00	26.20	41.80
Mg_2SiO_4							
0	20.17	37.82	29.13	11.76	1.12	0.00	0.00
5	13.17	37.82	32.21	13.73	2.66	0.42	0.00
10	9.24	22.83	33.75	22.97	8.12	2.80	0.28
15	6.58	22.97	28.57	23.53	12.04	6.02	0.28
20	2.94	12.32	26.89	28.15	18.35	9.52	1.82
25	1.96	9.94	21.15	27.03	22.97	13.59	3.36
30	1.54	7.84	16.67	27.31	23.81	18.07	4.76
40	1.12	4.62	15.55	25.91	26.05	19.47	7.14
60	0.56	3.22	9.66	23.39	26.19	25.91	10.64
80	0.42	2.52	10.36	19.33	26.61	26.47	13.87
100	0.42	2.38	9.52	15.97	27.87	26.75	16.25

The size distribution of the SiO_x-cluster is demonstrated in Table 8 ($MgSiO_3$) and Table 9 (Mg_2SiO_4). The size distribution of SiO_x drastically depends on pressure. Particularly, in Mg_2SiO_4 the glassy subnets have a small size, from several atoms to hundreds of atoms at ambient pressure. The model contains 144 separate SiO_4 units (5 atoms) (N_s = 144 atoms) and 37 clusters comprising two SiO_4 units (9 atoms). When the pressure increases, the subnets tend to merge to form the network. At 10 GPa, the network with 2176 atoms is formed. Besides, some small clusters containing 6 atoms (isolated SiO_5) or 10 atoms (SiO_4-SiO_5 clusters) also appear. At beyond pressure (20 – 100 GPa), the network consists of 3290 atoms, while small clusters are very few. It means that almost SiO_x clusters link to each other in the models.

Table 8. The size distribution of SiO_x clusters in $MgSiO_3$ at different pressures, where N_s is the number of clusters, N_a is the corresponding number of atoms in the cluster

0 GPa		5 GPa		10 GPa		20 GPa		40 GPa		100 GPa	
N_s	N_a	N_s	N_a	N_s	N_a	N_s	N_a	N_s	N_a	N_s	N_a
11	5	3	5	1	6	1	3860	1	3869	1	3890
1	6	1	3819	1	3831	-	-	-	-	-	-
2	9	-	-	-	-	-	-	-	-	-	-
1	13	-	-	-	-	-	-	-	-	-	-
1	3657	-	-	-	-	-	-	-	-	-	-

Table 9. The size distribution of SiO_x clusters in Mg_2SiO_4 at different pressures, where N_s is the number of clusters, N_a is the corresponding number of atoms in the cluster

0 GPa		10 GPa		20 GPa		40 GPa		60 GPa		100 GPa	
N_s	N_a	N_s	N_a	N_s	N_a	N_s	N_a	N_s	N_a	N_s	N_a
144	5	78	5	18	5	6	5	1	5	1	6
37	9	4	6	6	6	6	6	5	6	2	7
23	13	8	9	2	7	2	7	1	11	1	3296
8	17	5	10	2	9	2	11	1	3248	-	-
1	20	1	11	1	10	1	3166	-	-	-	-
2	21	1	13	1	14	-	-	-	-	-	-
1	22	4	14	1	17	-	-	-	-	-	-
1	24	11	17 – 62	1	29	-	-	-	-	-	-
6	25	1	2176	1	3012	-	-	-	-	-	-
2	28			-	-	-	-	-	-	-	-
2	29			-	-	-	-	-	-	-	-
16	30-249			-	-	-	-	-	-	-	-

In the meantime, in the $MgSiO_3$ model, at zero pressure, SiO_x units already link together to form a network of 3,657 atoms beside some small subnets. Because at low pressure, the proportion of BOs and Q^3 is dominant in $MgSiO_3$, while Mg_2SiO_4 model mainly consists of NBO and Q^1. Notably, in the pressure range 20 - 100 GPa, all SiO_x link to each other in the $MgSiO_3$ model. The size of SiO_x subnet at 100 GPa is larger than at 20 GPa because of the formation of higher coordinated polyhedrons. Hence, we can conclude that the polymerization of the glassy network occurs more significantly in Mg_2SiO_4 than in $MgSiO_3$.

Table 10 elucidates the size distribution of MgO_x subnets in both $MgSiO_3$ and Mg_2SiO_4 glass. As we can see, in $MgSiO_3$, several small units comprise 4- 16 atoms, (4 for MgO_3, 5 for MgO_4, 6 for MgO_5 and 7 for MgO_6 unit) and one network consists of 3251 atoms. In general, the MgO_x subnets are bigger than SiO_x subnets at the same pressure in both compounds because Mg-O has the higher coordination number than Si-O.

In $MgSiO_3$, all MgO_x units link to each other at the pressure of 5, 20, 40 and 100 GPa. While this phenomenon happens in the range of pressure (0 – 100 GPa) in Mg_2SiO_4. It is explained by the fact that the number of Mg atoms is twice as many as the number of Si atoms. The typical SiO_x subnets at 0 GPa and 10 GPa are illustrated in Figure 7.

Table 10. The size distribution of MgO_x clusters in both $MgSiO_3$ and Mg_2SiO_4 at different pressures, where N_s is the number of clusters, N_a is the corresponding number of atoms in the cluster

0 GPa		5 GPa		10 GPa		20 GPa		40 GPa		100 GPa	
N_s	N_a	N_s	N_a	N_s	N_a	N_s	N_a	N_s	N_a	N_s	N_a
1	4	1	3613	1	7	1	3781	1	3764	1	3845
3	5	-	-	1	3681	-	-	-	-	-	-
1	6	-	-	-	-	-	-	-	-	-	-
1	7	-	-	-	-	-	-	-	-	-	-
1	16	-	-	-	-	-	-	-	-	-	-
1	3251	-	-	-	-	-	-	-	-	-	-
1	4011	1	4114	1	4182	1	4243	1	4247	1	4267

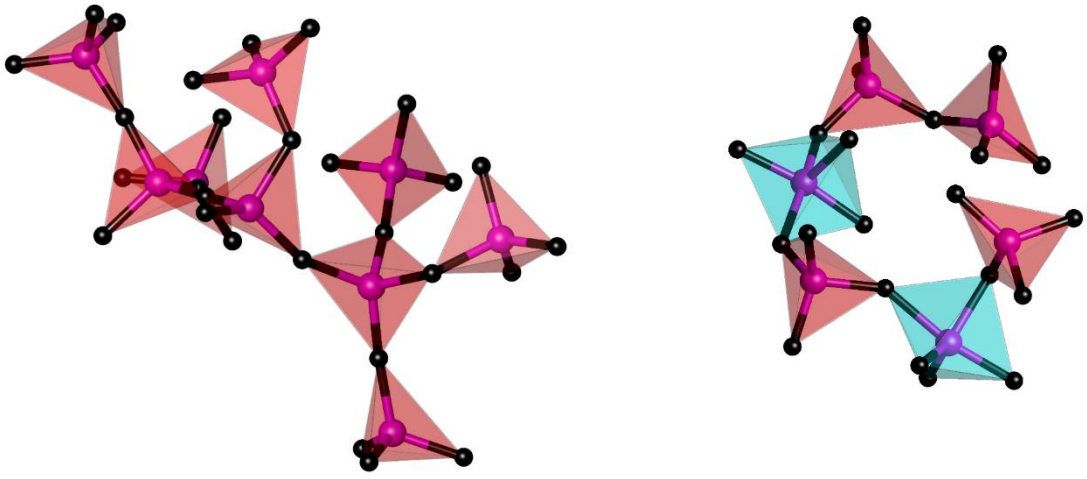

Figure 7. SiO_x cluster at ambient pressure (left) and 10 GPa (right). Si-O coordinated polyhedrons are color-coded, red for SiO_4 and cyan for SiO_5 units.

To clarify the connection of SiO_x units in the glassy network, the distribution of conner-, edge-, face-sharing subnets are investigated. Table 11 and Table 12 show the size distribution of edge-sharing and face-sharing subnets. At ambient pressure, there are several edge-sharing bonds in $MgSiO_3$, while this bond type is totally absent in Mg_2SiO_4 (see Table 3 and Table 11). We define that each edge-sharing bond is generated by 2 Si atoms, 2 bridging O atoms and the rested atoms in corresponding coordinated

polyhedrons (see Figure 8). Therefore, the subnets with N_a equal to 9 (or 10) are the isolated edge-sharing bonds. Under compression, at 10 GPa, the number of edge-sharing bonds increases (see Table 3). This helps the discrete edge-sharing bonds to link to each other in $MgSiO_3$ to create different subnets. The network consists of 1,584 atoms. At the same pressure, there is the existence of edge-sharing bonds with some isolated linkages. Then, at 40 GPa, isolated subnets are abundant in the model. Along with pressure growth, the more edge-sharing bonds are, the more they tend to link to each other to create the big subnets. Namely, at 40 GPa or higher, all edge-sharing bonds merge into one subnet in MgO-SiO glass. The network recorded at 100 GPa includes 3,568 atoms in $MgSiO_3$ and 1,795 atoms in Mg_2SiO_4. Regarding the face-sharing bond (see Table 12), at the low and intermediate (0-40 GPa) pressure, the proportion of face-sharing bonds is not significant (see Table 3), resulting in the very little appearance of face-sharing subnets. With the atom amount of 11 or 12 (see Figure 9), the face-sharing subnet is very small. Under densification, the number of face-sharing bonds goes up in both compounds, which leads to the creation of larger subnets. Even so, the small subnets remain existent. According to Table 12, in a general manner, we can recognize the merging tendency among face-sharing bonds. The biggest subnet of the face-sharing bond, which has 48 atoms in $MgSiO_3$ and 41 atoms in Mg_2SiO_4, is illustrated in Figure 10 (the red color represents the face-sharing bond). Figure 11 shows the comparison between the considered face-sharing subnet and the pure one (ignoring the atoms in basic units that are not involved in the bond).

Table 11. The size distribution of edge-sharing subnets under compression in $MgSiO_3$ and Mg_2SiO_4 (N_s is the number of clusters, N_a is the number of atoms in the corresponding cluster/subnet/network)

$MgSiO_3$											
0 GPa		10 GPa		20 GPa		40 GPa		60 GPa		100 GPa	
N_s	N_a	N_s	N_a	N_s	N_a	N_s	N_a	N_s	N_a	N_s	N_a
5	9	8	10	1	10	1	3,156	1	3,329	1	3,568
8	10	2	11	1	25	-	-	-	-	-	-
1	17	1	15	1	2,765	-	-	-	-	-	-
3	18	2	16	-	-	-	-	-	-	-	-
-	-	5	19 – 135	-	-	-	-	-	-	-	-
-	-	1	1,587	-	-	-	-	-	-	-	-
Mg_2SiO_4											
-	-	1	9	9	10	3	10	1	10	3	11
-	-	10	10	19	11	16	11	7	11	9	12
-	-	5	11	2	12	7	12	9	12	1	17
-	-	2	12	3	15	4	15	2	16	1	37
-	-	-	-	1	16	1	16	1	17	1	42
-	-	-	-	1	17	1	17	2	21	1	1,795
-	-	-	-	2	20	1	20	4	26 - 98	-	-
-	-	-	-	3	21	5	21-36	1	1,397	-	-
-	-	-	-	8	26 – 63	10	42 - 228	-	-	-	-

Table 12. The size distribution of face-sharing subnets under compression in $MgSiO_3$ and Mg_2SiO_4 (N_s is the number of clusters, N_a is the number of atoms in the corresponding cluster/subnet/network)

$MgSiO_3$											
0 GPa		10 GPa		20 GPa		40 GPa		60 GPa		100 GPa	
N_s	N_a	N_s	N_a	N_s	N_a	N_s	N_a	N_s	N_a	N_s	N_a
-	-	3	11	14	11	13	11	10	11	2	11
-	-	-	-	-	-	-	-	5	12	9	12
-	-	-	-	-	-	-	-	1	17	2	13
-	-	-	-	-	-	-	-	1	27	9	16-48
Mg_2SiO_4											
-	-	2	11	4	11	15	11	15	11	18	11
-	-	-	-	-	-	-	-	1	15	1	12
-	-	-	-	-	-	-	-	-	-	1	31
-	-	-	-	-	-	-	-	-	-	1	41

Figure 8. The typical small edge-sharing subnet of 11 atoms (left) and 15 atoms (right).

Figure 9. The typical small face-sharing subnet of 11 atoms (left) and 12 atoms (right).

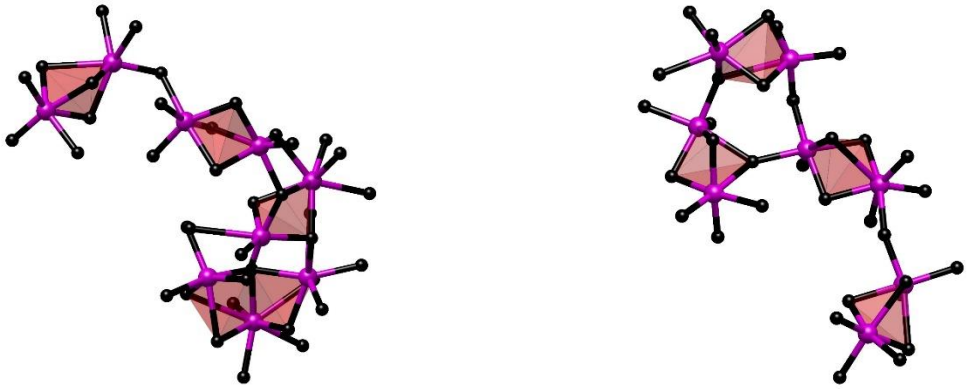

Figure 10. The broadest face-sharing subnet of 48 atoms in $MgSiO_3$ (left) and 41 atoms in Mg_2SiO_4 (right).

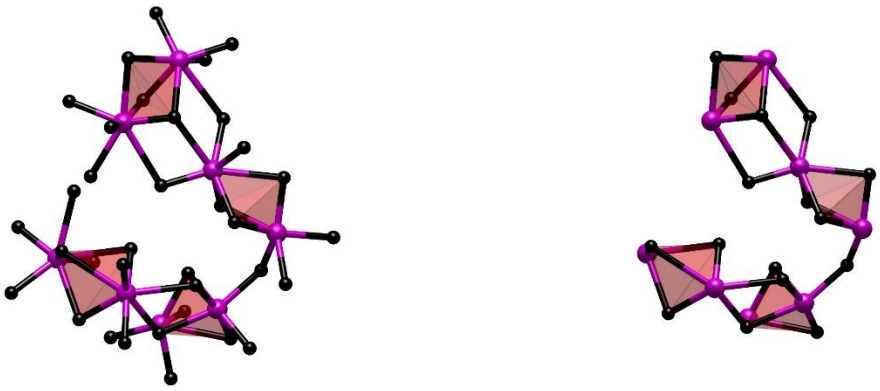

Figure 11. The face-sharing subnet and pure one comprising atoms in face-sharing bond.

Along with the pressure increase, the Mg^{2+} ions tend to connect with the glassy network, forming the large subnet or Mg-Si network in the model. In addition to distribution analysis on BOs and NBOs, the corner-, edge-, and face-sharing bonds are analyzed and visualized to illuminate the Mg^{2+} incorporation into the glassy network. When we take the rest atoms in the coordinated polyhedron into account, we have the size distribution results as in and a visualization of the typical subnet of Mg-Si face-sharing bond as in Figure 12.

Table 13. Size distribution of Mg-Si edge-sharing subnets/network under densification.

$MgSiO_3$									
0 GPa		5 GPa		10 GPa		20 GPa		100 GPa	
N_s	N_a	N_s	N_a	N_s	N_a	N_s	N_a	N_s	N_a
4	7	1	4,751	1	4,855	1	4,889	1	4,946
8	8	-	-	-	-	-	-	-	-
4	9	-	-	-	-	-	-	-	-
1	10	-	-	-	-	-	-	-	-
11	11-20	-	-	-	-	-	-	-	-
6	21-34	-	-	-	-	-	-	-	-
1	100	-	-	-	-	-	-	-	-
1	152	-	-	-	-	-	-	-	-
1	2,108	-	-	-	-	-	-	-	-
Mg_2SiO_4									
1	7	2	8	1	3,997	1	4,522	1	4,819
10	8	2	9	-	-	-	-	-	-
20	9	1	17	-	-	-	-	-	-
6	10	1	3,300	-	-	-	-	-	-
8	11-20	-	-	-	-	-	-	-	-
5	21-40	-	-	-	-	-	-	-	-
1	47	-	-	-	-	-	-	-	-
1	1,701	-	-	-	-	-	-	-	-

Table 14. Size distribution of Mg-Si face-sharing subnets/network under densification

$MgSiO_3$									
0 GPa		20 GPa		40 GPa		60 GPa		100 GPa	
N_s	N_a	N_s	N_a	N_s	N_a	N_s	N_a	N_s	N_a
1	9	1	9	1	9	5	9	1	3,441
3	10	6	10	6	10	8	11-20	-	-
-	-	27	11-20	8	11-20	2	21	-	-
-	-	11	21-60	11	21-60	1	69	-	-
-	-	1	64	2	61-100	1	2,136	-	-
-	-	1	76	1	125	-	-	-	-
-	-	-	-	1	131	-	-	-	-
-	-	-	-	1	166	-	-	-	-
-	-	-	-	1	536	-	-	-	-
Mg_2SiO_4									
-	-	2	9	1	10	1	12	1	3,853
-	-	7	10	6	11	1	3,257	-	-
-	-	22	11-20	1	12	-	-	-	-
-	-	6	21-60	1	21	-	-	-	-
-	-	4	61-200	1	2,511	-	-	-	-
-	-	1	202	-	-	-	-	-	-
-	-	1	209	-	-	-	-	-	-
-	-	1	220	-	-	-	-	-	-

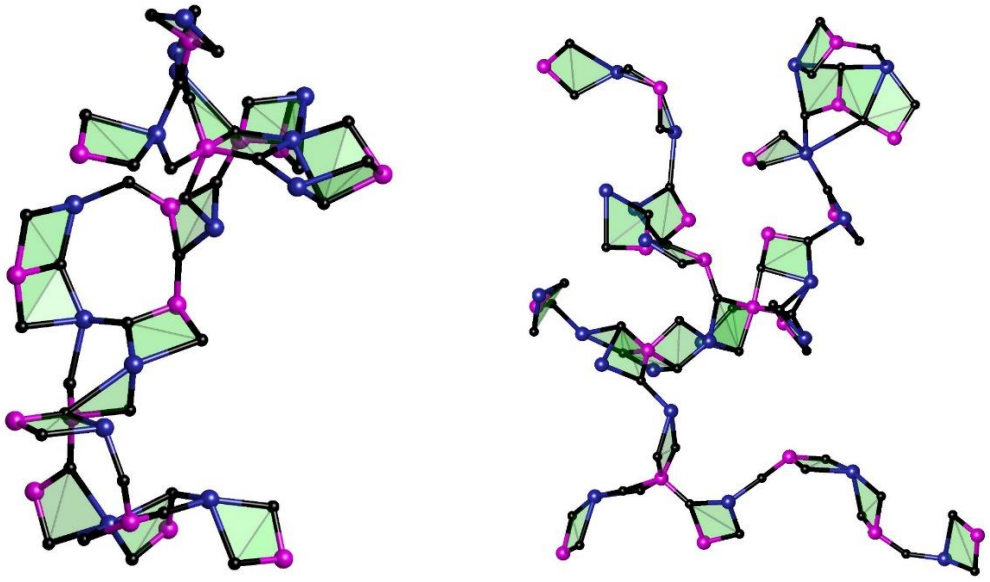

Figure 12. Mg-Si subnet comprising 100 atoms (left) and 152 atoms (right). Magnetic, pink, black is Mg, Si, O species, respectively.

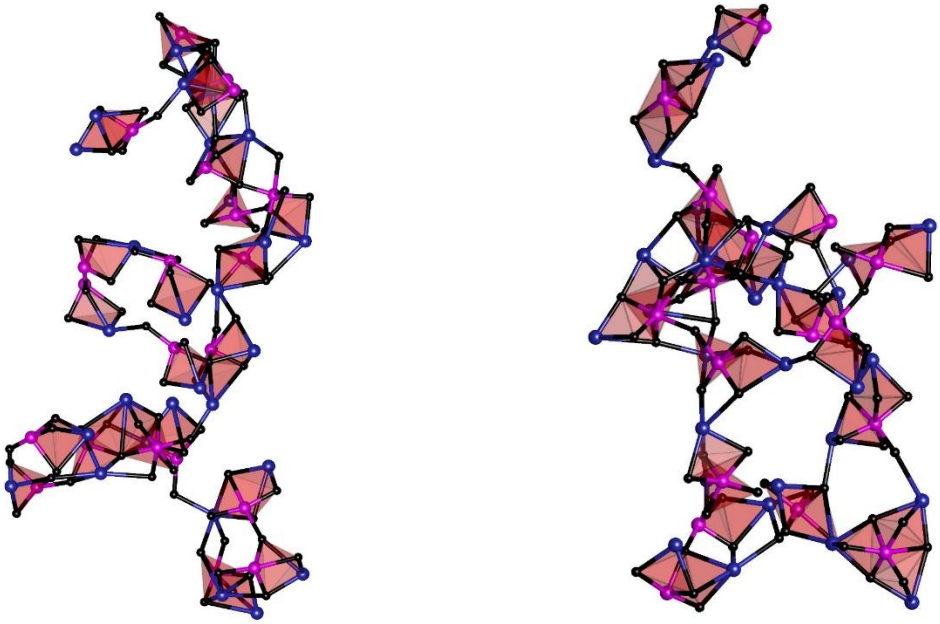

Figure 13. The Mg-Si subnet comprising 220 atoms (left) and 209 atoms (right). Magnetic, pink, black is Mg, Si, O species, respectively.

Table 13 and Table 14 present the size distribution of Mg-Si edge-sharing subnets/network and face-sharing subnets/network. It is obvious that Mg^{2+} ions link to -Si-O- network through corner-sharing bonds at ambient pressure (see Table 5). At the same condition, the atom amount of the edge-sharing network accounts for about two-fifths of entire atoms in both materials. In the meantime, face-sharing bonds are very few in $MgSiO_3$ and totally absent in Mg_2SiO_4. As a result, Mg^{2+} ions link to -Si-O- subnet via one common O atom to form corner sharing subnets that are larger than edge- or face-sharing subnets. At higher pressure, the numbers of edge-sharing and face-sharing bonds increase. At 5 GPa, almost Mg-Si sharing bonds in the model link to each other. Regardless of any pressure, the edge-sharing network in $MgSiO_3$ are always larger than the one in Mg_2SiO_4 model. Because the proportion of statistical edge-sharing bonds in $MgSiO_3$ is higher than Mg_2SiO_4. In contrast, although Mg-Si face-sharing does not appear at 0 GPa in Mg_2SiO_4, the face-sharing network of Mg-Si in the Mg_2SiO_4 contain more atoms than the one in $MgSiO_3$ at the higher-pressure interval. The distribution of clusters is very diverse with the size ranging from several to hundreds of atoms (40 GPa for $MgSiO_3$, 20 GPa for Mg_2SiO_4) or thousands of atoms (60 GPa for $MgSiO_3$, 40 GPa for Mg_2SiO_4). At 20 GPa, the largest subnet includes 76 atoms in $MgSiO_3$ and 220 atoms in Mg_2SiO_4. At higher pressure, the face-sharing bonds merge in both compounds. All face-sharing bonds in two compounds merge into one face-sharing network of 3441 atoms in $MgSiO_3$ and 3853 atoms in Mg_2SiO_4. Figure 13 illustrates a typical Mg-Si subnet at 20 GPa in Mg_2SiO_4.

4. Conclusion

The size distribution of SiO_x drastically depends on pressure. At ambient pressure, the glassy subnets in Mg_2SiO_4 have small sizes, from several atoms to hundreds of atoms. Those subnets link to each other mostly via one common atom (bridge-oxygen). Because the fraction of FOs in the models accounts for a considerable quantity, the large Mg-rich region contains isolated small SiO_x units or small clusters.

This proves the heterogeneous structure in $MgSiO_3$ and Mg_2SiO_4. The number of FOs in Mg_2SiO_4 is larger than that in $MgSiO_3$. As a result, the Mg_2SiO_4 model is more non-uniform than $MgSiO_3$ model. Under compression, basic units tend to merge to form the bigger subnets/network. Almost SiO_x and MgO_x units link to each other in the models due to the establishment of higher coordinated species and the appearance of BO. This work also analyses the distribution of Q^n to clarify the degree of polymerization of -Si-O- glassy network. Based on that, one can conclude that the glassy network in the $MgSiO_3$ model has a higher degree of polymerization than in Mg_2SiO_4 model. Under densification, there are linkage transitions among Si-Si and Mg-Si species. At ambient pressure, Si species link with another Si via the corner-sharing bond. It is similar to the way that Mg links to the -Si-O- glassy network. At higher pressure, edge- and face-sharing bonds increase. The linkages of Si-Si and Mg-Si become rich sets of corner-, edge- and face-sharing bonds. The distributions of linkages are non-uniform but tend to form clusters. The spatial distributions of these linkages in both compounds are also depicted in three-dimension to illuminate the heterogeneous property. There is a change in incorporation mechanism of Mg^{2+} ions into the -Si-O- glassy network. At ambient pressure, almost Mg^{2+} ions link to the -Si-O- network via NBOs in Mg_2SiO_4 and via both NBOs and BOs in $MgSiO_3$. Besides, the Mg^{2+} ions also connect to the glassy network through corner-sharing bonds in both ternary materials. In Mg_2SiO_4 with the high range of pressure, by virtue of the few FOs existence, the Mg species link to the -Si-O- network via mainly NBOs and BOs. However, under the same condition, NBO in $MgSiO_3$ account for a low proportion. Therefore, Mg^{2+} ions link to -Si-O- network commonly through BOs. Due to the formation of abundant edge-sharing and face-sharing bonds between Mg-Si, the Mg^{2+} ions have the tendency to incorporate with -Si-O- network via all three bond types, although the distribution of edge-sharing and face-sharing bonds is not uniform. In combination with the above analysis, the subnets/network established from corner-, edge-, face-sharing bonds and SiO_x units are apparently and specifically visualized. The illustrations concerning ternary compounds are also displayed distinctly. Hence, the readers can find it easy to imagine and monitor the transitions of these linkages and the formation of the subnets/clusters.

Acknowledgement

This simulation is carried out on the high-performance computing system in RIKEN. Representative laboratory at RIKEN: RIKEN Cluster for Pioneering Research, Theoretical Quantum Physics Laboratory and RIKEN Center for Computational Science, Discrete Event Simulation Research Team.

This research is performed with the support of Hanoi University of Science and Technology.

References

[1] A. Yamada, S. J. Gaudio, C. E. Lesher, Densification of $MgSiO_3$ Glass with Pressure and Temperature, J. Phys. Conf. Ser., Vol. 215, 2010, pp. 6-11, https//doi.org/10.1088/1742-6596/215/1/012085.

[2] D. B. Ghosh, B. B. Karki, Diffusion and Viscosity of Mg_2SiO_4 Liquid at High Pressure from First-Principles Simulations, Geochim. Cosmochim. Acta, Vol. 75, No. 16, 2011, pp. 4591-4600, https//doi.org/10.1016/J.Gca.2011.05.030.

[3] D. B. Ghosh, B. B. Karki, First Principles Simulations of the Stability and Structure of Grain Boundaries in Mg_2SiO_4 Forsterite, 2014, pp. 163-171, https//doi.org/10.1007/S00269-013-0633-1.

[4] R. M. Bolis et al., Decaying Shock Studies of Phase Transitions in MgO-SiO_2 Systems: Implications for the Super-Earths' Interiors, Geophys. Res. Lett., Vol. 43, No. 18, pp. 9475-9483, 2016, https//doi.org/10.1002/2016gl070466.

[5] O. Adjaoud, G. S. Neumann, S. Jahn, Mg_2SiO_4 Liquid Under High Pressure from Molecular Dynamics, Chem. Geol., Vol. 256, No. 3-4, 2008, pp. 184-191, https//doi.org/10.1016/J.Chemgeo.2008.06.031.

[6] J. T. K. Wan, T. S. Duffy, S. Scandolo, R. Car, First Principles Study of Density, Viscosity, and Diffusion Coefficients of Liquid $MgSiO_3$ at Conditions of the Earth's Deep Mantle, J. Geophys. Res., Vol. 112, No. B3, 2005, pp. 1-6, https//doi.org/10.1029/2005jb004135.

[7] W. H. Zachariasen, The Atomic Arrangement in Glass, J. Am. Chem. Soc., Vol. 54, No. 10, 1932, pp. 3841-3851, https//doi.org/10.1021/Ja01349a006.

[8] L. Cormier, G. J. Cuello, Mg Coordination in A $MgSiO_3$ Glass Using Neutron Diffraction Coupled with Isotopic Substitution, Phys. Rev. B, Vol. 83, 2011, pp. 224204, https//doi.org/10.1103/Physrevb.83.224204.

[9] M. C. Wilding, C. J. Benmore, J. K. R. Weber, In Situ Diffraction Studies of Magnesium Silicate Liquids, 2008, pp. 4707-4713, https//doi.org/10.1007/S10853-007-2356-5.

[10] A. G. Kalampounias, N. K. Nasikas, G. N. Papatheodorou, Glass Formation and Structure in the Mgsio3 – Mg2sio4 Pseudobinary System: from Degraded Networks to Ioniclike Glasses Glass Formation and Structure in the Mgsio3 – Mg_2SiO_4 Pseudobinary System: from Degraded Networks to Ioniclike Glasses, J. Chem. Phys., Vol. 114513, No. 131, 2009, pp. 114513, https//doi.org/10.1063/1.3225431.

[11] C. D. Yin, M. Okuno, H. Morikawa, F. Marumo, Structure Analysis of $MgSiO_3$ Glass, J. Non. Cryst. Solids, Vol. 55, 1983, pp. 131-141, https//doi.org/10.1016/0022-3093(83)90013-3.

[12] J. B. Haskins, E. C. Stern, C. W. Bauschlicher, J. W. Lawson, Thermodynamic and Transport Properties of Meteor Melt Constituents from Ab Initio Simulations: $MgSiO_3$, SiO_2, and MgO, J. Appl. Phys., Vol. 125, No. 23, 2019, https//doi.org/10.1063/1.5079418.

[13] R. K. Kalia, A. Nakano, P. Vashishta, Structure of Rings in Vitreous SiO_2, Phys. Rev. B, Vol. 47, No. 6, 1993, pp. 3053-3062, https//doi.org/10.1103/Physrevb.47.3053.

[14] B. M. A. Hasni, G. Mountjoy, A Molecular Dynamics Study of the Atomic Structure of X(Mgo) 100−X(Sio2), J. Non. Cryst. Solids, Vol. 400, 2014, pp. 33-44, https//doi.org/10.1016/J.Jnoncrysol.2013.11.011.

[15] S. Kohara et al., Glass Formation at the Limit of Insufficient Network Formers, Science, Vol. 303, No. 5664, 2004, pp. 1649-1652, https//doi.org/10.1126/Science.1095047.

[16] C. J. Benmore et al., High Pressure X-Ray Diffraction Measurements on Mg_2SiO_4 Glass, J. Non. Cryst. Solids, Vol. 357, No. 14, 2011, pp. 2632-2636, https//doi.org/10.1016/J.Jnoncrysol.2010.12.064.

[17] C. J. Benmore et al., Structural and Topological Changes in Silica Glass at Pressure, Phys. Rev. B - Condens. Matter Mater. Phys., Vol. 81, No. 5, 2010, pp. 1-5, https//doi.org/10.1103/Physrevb.81.054105.

[18] N. H. Son, N. H. Anh, P. H. Kien, T. Iitaka, N. V. Hong, P. Huu, Topology of Siox-units and Glassy Network of Magnesium Silicate Glass under Densification: Correlation Between Radial Distribution Function and Bond Angle Distribution, Model. Simul. Mater. Sci. Eng., Vol. 28, No. 6, 2020, pp. 065007, https//doi.org/10.1088/1361-651x/Ab9bb4.

[19] A. R. Oganov, J. P. Brodholt, G. D. Price, Comparative Study of Quasiharmonic Lattice Dynamics, Molecular Dynamics and Debye Model Applied to $MgSiO_3$ Perovskite, Phys. Earth Planet. Inter., Vol. 122, No. 3-4, 2000, pp. 277-288, https//doi.org/10.1016/S0031-9201(00)00197-7.

[20] A. M. Goryaeva, P. Carrez, P. Cordier, Modeling Defects and Plasticity in $MgSiO_3$ Post - Perovskite : Part 2 - Screw and Edge [100] Dislocations, Phys. Chem. Miner., Vol. 42, No. 10, 2015, pp. 793-803, https//doi.org/10.1007/S00269-015-0763-8.

[21] Z. Liu, C. Zhang, X. Sun, J. Hu, T. Song, Y. D. Chu, The Melting Curve of $MgSiO_3$ Perovskite from Molecular Dynamics Simulation, Phys. Scr., Vol. 83, 2011, pp. 045602, https//doi.org/10.1088/0031-8949/83/04/045602.

[22] D. Nevins, F. J. Spera, M. S. Ghiorso, Shear Viscosity and Diffusion in Liquid $MgSiO_3$: Transport Properties and Implications for Terrestrial Planet Magma Oceans, Am. Mineral., Vol. 94, No. 7, 2009, pp. 975-980, https//doi.org/10.2138/Am.2009.3092.

[23] F. J. Spera, M. S. Ghiorso, D. Nevins, Structure, Thermodynamic and Transport Properties of Liquid $MgSiO_3$: Comparison of Molecular Models and Laboratory Results, Geochim. Cosmochim. Acta, Vol. 75, No. 5, 2011, pp. 1272-1296, https//doi.org/10.1016/J.Gca.2010.12.004.

[24] S. Kohara et al., Relationship Between Topological Order and Glass Forming Ability in Densely Packed Enstatite and Forsterite Composition Glasses, Proc. Natl. Acad. Sci., Vol. 10, No. 108, 2011, pp. 14780-14785, https//doi.org/10.1073/Pnas.1104692108/-/Dcsupplemental.Www.Pnas.Org/Cgi/Doi/10.1073/Pnas.1104692108.

[25] M. C. Wilding, C. J. Benmore, J. A. Tangeman, S. Sampath, Evidence of Different Structures in Magnesium Silicate Liquids: Coordination Changes in Forsterite- to Enstatite-Composition Glasses, Vol. 213, 2004, pp. 281-291, https//doi.org/10.1016/J.Chemgeo.2004.08.055.

[26] J. D. Kubicki, A. C. Lasaga, Molecular Dynamics Simulations of Pressure and Temperature Effects on $MgSiO_3$ and Mg_2SiO_4 Melts and Glasses, Phys. Chem. Miner., Vol. 17, 1991, pp. 661-673, https//doi.org/10.1016/J.Epsl.2010.04.034.

[27] S. Kohara, K. Suzuya, High-Energy X-Ray Diffraction Studies of Disordered Materials, Nucl. Instruments Methods Phys. Res. Sect. B Beam Interact, with Mater. Atoms, Vol. 199, 2003, pp. 23-28, https//doi.org/10.1016/S0168-583x(02)01554-9.

[28] N. T. Nhan, G. Thi, T. Trang, T. Iitaka, N. V. Hong, Crystallization of Amorphous Silica Under Compression, Can. Sci. Publ., Vol. 97, No. 10, 2019, pp. 20-29, https//doi.org/10.1139/Cjp-2018-0432.